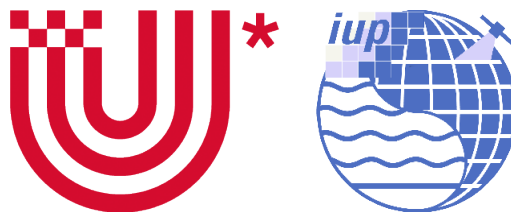


# SCIAMACHY V8 UV Radiance Validation Using a Soft-Calibration Approach

**Stefan Bötzel, Mark Weber, John P. Burrows**  
Institut für Umweltphysik, Universität Bremen, Bremen, Germany

Document Number : SCILOV-15-IUP-UVR-ScV-TN  
Version : 2.0  
Date : October 7, 2016  
Contact : Mark Weber (weber@uni-bremen.de)  
Universität Bremen FB1  
P.O. Box 330 440  
D-28334 Bremen  
Status : Final



# Contents

1	Introduction . . . . .	3
2	Soft calibration . . . . .	4
2.1	Initial calibration . . . . .	5
2.2	Monthly calibration . . . . .	5
2.3	Setup of the radiative transfer model . . . . .	6
2.4	Choice of geographical regions . . . . .	6
3	Results for SCIAMACHY V7 radiances . . . . .	7
3.1	Results for SCIAMACHY I1b V7 without m-factors applied . . . . .	7
3.2	Results for SCIAMACHY I1b V7 with m-factors applied . . . . .	13
4	Results for SCIAMACHY V8 radiances . . . . .	15
5	Comparisons between V7 and V8 based on different scan-angles . . . . .	19
5.1	Ground pixel no. 1 . . . . .	19
5.2	Ground pixel no. 2 . . . . .	21
5.3	Ground pixel no. 3 . . . . .	23
5.4	Ground pixel no. 4 . . . . .	25
6	Executive summary . . . . .	27
7	References . . . . .	28

## 1 Introduction

The quality of measured radiances from any space borne instrument is generally dependent on its precision and accuracy. Over time it can be expected that both precision and accuracy will decrease. A decrease in accuracy can be generally considered to be caused by instrument degradation, such as a buildup of matter on optical components, which can have a severe effect on the quality of the measured data and thus on products retrieved using measured spectra.

Instrument degradation in the ultraviolet spectral region was already identified as an issue for the BUUV instrument (Jaross et al., 1998) and particularly for long-term and multi-instrument datasets a good correction of the degradation effects is vital. An incorrect handling of degradation effects has already been shown to have a severe impact on the derivation of long term trends of zone data products (Herman et al., 1991, 1990).

Additionally uncertainties in the initial calibration can have a large impact on the retrieved ozone profiles (Janz et al., 1995). A large part of the degradation in BUUV was attributed to contamination of the solar diffuser. The latter is used to achieve the full illumination of the entrance aperture by the extraterrestrial solar radiation. To account for the degradation of the BUUV data as well as SBUV (Nimbus-7) data, all SBUV/2 instruments from NOAA-9a onwards included a mercury lamp which was viewed directly and via the diffuser (Hilsenrath et al., 1997). Additionally the spectral discrimination method (Hilsenrath et al., 1997) or a simplification thereof called pair justification method (Herman et al., 1991) can be used for a calibration correction assuming that degradation occurs at a linear rate.

Another approach is the inter-comparison between different satellite instruments and the SSBUV (Shuttle SBUV) instrument (Frederick et al., 1990). For this approach an optically identical instrument was carried by a space shuttle orbiter. On the ground an extensive calibration before and after shuttle launch was carried out in order to determine the uncertainty in the SSBUV comparisons in space. Additionally there are methods based on average photomultiplier tube counts as outlined in Taylor et al. (2003).

Furthermore a soft calibration based on the comparison of radiances with expected values for the snow/ice albedo has been proposed by DeLand et al. (2004). Such a vicarious calibration technique (as outlined in Campbell (1982)), often also referred to as "soft calibration", focuses on recalibrating radiances by comparing them to modelled radiances thus correcting for changes in the instrument as a whole whereas "hard" calibration techniques usually attempt to separate observed changes into effects for the different optical components inside the instrument yielding a physical model for a possible recalibration. This method has been further developed and applied to SBUV spectra for the version 8.6 SBUV ozone data product (DeLand et al., 2012). DeLand et al. (2012) also use this soft calibration to evaluate the pre-launch calibration showing a disagreement of up to 12%.

A soft calibration approach based on the comparison of observed radiances with expected values over the Libyan Desert was reported by Krijger et al. (2007). This study also proposes an initial recalibration for the GOME instrument based on a fairly constant degradation function for the first two years of operation. Liu and Chance (2007) describe a calibration method where the ratio between the deseasonalised average reflectance between 60°N and 60°S for any given time and the beginning of the mission is used. The impact of the calculated degradation on retrieved ozone profiles is also shown to be large.

A comprehensive long-term analysis of the instrument degradation for GOME has been provided by Coldewey-Egbers et al. (2008) and Krijger et al. (2005) showing a 20% to 50% degradation in the UV below 305 nm in 2003 after eight years in orbit.

For SCIAMACHY the degradation correction can be performed for each viewing geometry by apply-

ing specific monitoring factors (m-factors) (Noël et al., 2003), which are calculated from unobstructed sun or moon observations as described in Bramstedt (2008). These m-factors however only correct for changes from the first day of measurement onwards. Even at the start of the mission changes in the radiances from the pre-flight calibration made on ground are evident (Gottwald et al., 2011).

Overall it can be expected that instruments measuring in the UV range degrade over time due to the hard radiation polymerising optical surfaces. For the SBUV instruments the cause of degradation is believed to be changes in the diffuser plate, while contaminants on the external mirror redirecting radiation into the spectrometer are the main cause for GOME type instruments (Krijger et al., 2014). The degradation rate differs between instruments and depends on the actual exposure.

Most in-flight calibration and degradation correction techniques can be seen as “hard” calibration and are usually designed specifically for one instrument. These techniques generally provide very good results but have the drawback that once a new effect is found to be occurring in the optical set-up of an instrument much consideration has to be given to understanding the actual effect before a proper correction can be found. In contrast the “soft” calibration techniques above, do not need detailed knowledge of the instrument calibration history, however, they require some time before they can be performed because of the large sampling needed. Furthermore often they only treat changes of the instrument relative to some initial state.

A soft calibration technique usable from the beginning of the mission for various nadir viewing UV spectrometers is presented in Section 2 with spectral corrections for SCIAMACHY level 1b V7 shown in Section 3 and an update using I1b V8 shown in Section 4.

## 2 Soft calibration

This soft calibration is based on the comparison of measured radiances with expected values, simulated using radiative transfer as outlined in Section 2.3, in a similar manner as used by Krijger et al. (2007). Measured radiances are here defined as the ratio of the nadir spectrum to the direct solar irradiance measurements (“sun-normalized radiance”). The main differences are the choice of regions, the use of monthly means and the separation into an initial (post-launch) and a continuous (time-varying) part. All corrections are based on calculating the ratio between actual measured radiances and expected values as calculated from forward radiative transfer simulations (Section 2.3) over three specific regions (Section 2.4). The calibration correction  $c$  is determined for every wavelength  $\lambda_j$  in the wavelength window vector  $\vec{\lambda}$  so that:

$$c(\lambda_j) = \frac{s(\lambda_j)}{m(\lambda_j)} \quad (1)$$

where  $s(\lambda_j)$  is the simulated expected radiance at wavelength  $\lambda_j$  and  $m(\lambda_j)$  is the corresponding measured radiance. Assuming that the mean state of the atmosphere is reasonably well represented by the ozone profile climatology used in the radiative transfer model (see Section 2.3), the observed mean sun-normalised radiance in a given region and month should roughly equal the mean simulated radiance using climatologically ozone profiles. The corrected radiance  $r$  can be calculated from the measured radiance as

$$r(\lambda_j) = c(\lambda_j) \cdot m(\lambda_j) \quad (2)$$

where  $c(\lambda_j)$  is determined by taking the monthly mean of individual corrections. In general we distinguish between three types of calibration correction. An initial calibration correction  $c_0$  (Section 2.1) representing changes between pre-launch and post-launch state, a calibration correction  $c_m$  (Section 2.1) that varies with time, and represents the in-orbit change in the calibration or degradation. The

total correction ( $c$ ) is given by the product of ( $c_0$ ) and ( $c_m$ ). The advantage of splitting up the calibration correction into a fixed part and a part changing with time is that the variable contribution  $c_m$  can easily be compared to existing degradation correction schemes like the SCIAMACHY  $m$ -factors which do not account for immediate post-launch changes in the calibration. In all cases a single measured spectrum is used. This leads to channels with a shorter integration being co-added to the longest integration time (usually Band 1A). The scan angle dependence (for integration times of 1.5 sec corresponding to four ground pixels across the scan) is investigated in Section 5.

## 2.1 Initial calibration

The initial calibration correction  $c_0$  is essentially the calibration correction  $c$  for the first month of measurements.  $N$  pixels are chosen for each region  $i$  so that for wavelength  $\lambda_j$

$$c_{0,i}(\lambda_j) = \frac{1}{N} \sum_{n=1}^N \frac{s_{i,n}(\lambda_j)}{m_{i,n}(\lambda_j)} \quad (3)$$

and

$$c_0(\lambda_j) = \frac{1}{3} \sum_{i=1}^3 c_{0,i}(\lambda_j) \quad (4)$$

where  $s$  is the simulated radiance and  $m$  the measured radiance.  $c_0$  is then averaged over the three target regions on earth outlined in Section 2.4 and afterwards smoothed along the wavelength axis with a 10 point boxcar function ( 1.1 nm). As the possibility of a rapid degradation can not be excluded the initial calibration correction is done for a relatively small number of ground scenes over a limited duration. Compared to other recalibration techniques, such as shown in Krijger et al. (2007) this leads to some noise in the spectral domain in each region in  $c_0$  on top of the scatter expected due to natural variability. Overall this method is comparable to the one described in Krijger et al. (2007) with the main difference being that in our method the radiance is computed instead of the reflectance. It is however straightforward to convert radiance  $I$  to reflectance  $R$  using the formula

$$R = \frac{\pi I}{E_0 \mu_0} \quad (5)$$

where  $E_0$  is the solar irradiance and  $\mu_0$  is the cosine of the solar zenith angle. As this is merely a multiplicative operation  $c_0$  should be comparable to the results from Krijger et al. (2007). This method is also similar to the snow/ice radiance method for testing the post-launch calibration for SBUV-type instruments described in DeLand et al. (2012). However as this method is applied to SBUV-type instruments it only uses selected wavelengths.

## 2.2 Monthly calibration

The monthly calibration correction  $c_m$  is calculated in a very similar way to  $c_0$ . However  $c_0$  is first applied to the measured radiances according to equation 2 when calculating the corrections for each month.

$$c_{m,i}(\lambda_j) = \frac{1}{N'} \sum_{n=1}^{N'} \frac{s_{i,n}(\lambda_j)}{c_0(\lambda_j) \cdot m_{i,n}(\lambda_j)} \quad (6)$$

and

$$c_m(\lambda_j) = \frac{1}{3} \sum_{i=1}^3 c_{m,i}(\lambda_j) \quad (7)$$

This leads to the absolute calibration correction being

$$C = C_0 \cdot C_m \quad (8)$$

for each month. Due to the small number of pixels used every month as opposed to evaluating a whole year rapid changes in the detector can be found and accounted for quickly. This method, if averaged over a year, is comparable to the recalibration shown in Krijger et al. (2007).

### 2.3 Setup of the radiative transfer model

In this study the radiative transfer model (RTM) SCIATRAN (Rozanov et al., 2014) is used to simulate the sun-normalised radiance spectra used in the soft calibration. The pressure and temperature profiles are taken from ECMWF ERA-Interim (Dee et al., 2011) data while the assumed O<sub>3</sub>-profile is constructed from the IUP O<sub>3</sub>-climatology (Lamsal et al., 2004) scaled to retrieved WFDOAS O<sub>3</sub> total columns (Coldewey-Egbers et al., 2005; Weber et al., 2005). The spectral albedo, as defined in Kondratiev et al. (1964), is taken from the Guzzi database (Guzzi et al., 1996). Geometry parameters such as latitude, longitude, viewing and solar zenith angles are prescribed by the instrument. The expected radiance is modelled for the instrumental wavelength grid, the instrument slit function applied, and then compared to the observed and measured sun-normalised radiance from SCIAMACHY. The comparison is only meaningful when done using a large sample of radiances in the selected regions (next Section).

### 2.4 Choice of geographical regions

Three regions (as shown in Fig. 1) were chosen to perform the simulation of radiance spectra. These were two Pacific regions between 180W and 140W with 0N-10N and 40S-30S. Additionally the Antarctic region between 70S and 80S was used. These regions were chosen because on one hand the ground albedo is fairly well known as either snow (high albedo) or open water (low albedo) and on the other hand these regions have a large enough variability of parameters like temperature, pressure and O<sub>3</sub> profiles as well as solar zenith angles so that small discrepancies especially in the climatological data will play a limited role once the correction spectra are averaged. Only measurements that have a cloud fraction of less than 1% were used in order to avoid additional uncertainties from modelling the clouds in the radiative transfer calculations. These ground pixels are considered to be completely cloud free to minimise the uncertainty due to cloud albedo and cloud top height and to ensure that possible dark or bright biases are visible when comparing results for the three target regions. For the initial correction spectrum  $c_0(\lambda)$  all pixels within the described regions of the first month of measurement of the particular satellite instrument were used. For the monthly correction spectrum  $c_m(\lambda)$  a set of approximately 100 evenly spaced cloud free pixels from the first 10 days of each month were used in each region.

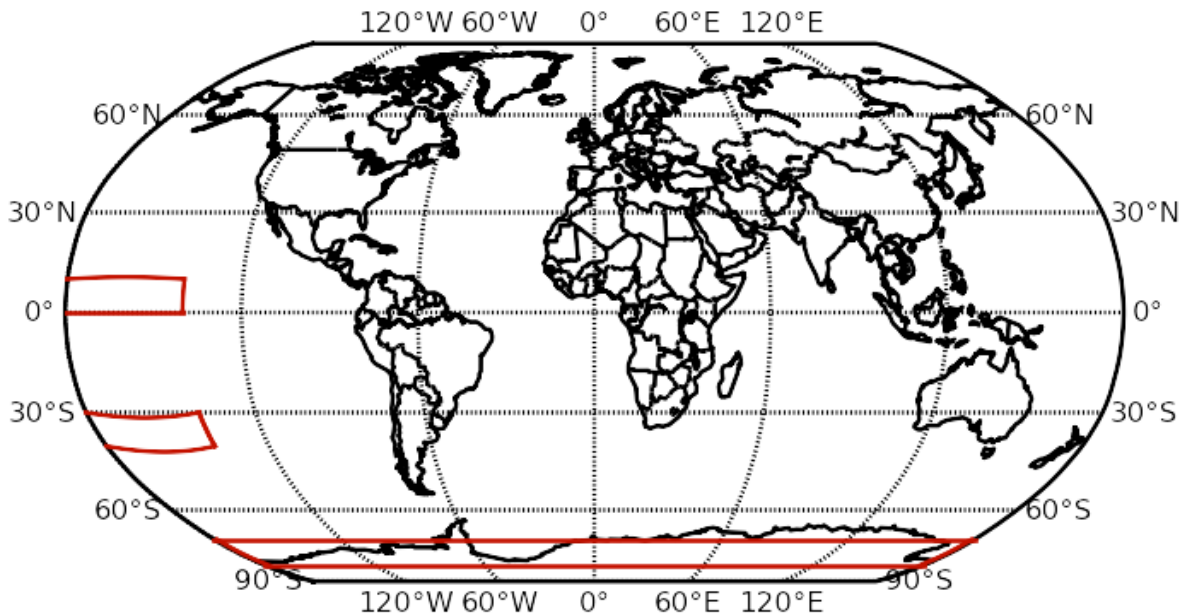


Figure 1: Map showing the three regions used in the soft calibration.

### 3 Results for SCIAMACHY V7 radiances

#### 3.1 Results for SCIAMACHY I1b V7 without m-factors applied

Figure 2 a shows the initial soft calibration for SCIAMACHY. It is evident that there is a large discrepancy between channel 1 below 303 nm and channel 2 from 303 nm onwards. While there are slight differences between the three regions the overall pattern is the same. A feature, which is immediately evident is the increased scatter at higher latitudes. Two effects may be responsible for this scatter. On one hand the number of spectra used is lower at high latitudes (47 for the latitudes from 70S to 80S, 179 for latitudes 40S to 30S and 223 for latitudes 0N to 10N for August 2002). On the other hand the variability of ozone, temperature and pressure prescribed in the RTM simulation is larger for mid and high latitudes than the tropics. These effects are negligible after applying a 10 point boxcar smoothing as shown by the thick curves. There are no systematic differences between the three regions. This implies that averaging the correction spectra from the three target regions results in a negligible error. Overall it can be seen that for channel 1 radiances are initially overestimated by approximately 25-30%. The majority of channel 2 shows radiances that are very close to the simulated. Between 300 and 310 nm (near the channel boundaries) there is a rapid change of the calibration factors going from near 1 to 0.7 with decreasing wavelengths.

The evolution of the instrument degradation is shown in Figure 3 for seasonal averages from August to October (ASO), November to January (NDJ), February to April (FMA) and May to July (MJJ). Larger and faster degradation occurs towards smaller wavelengths, which is expected from the increased energy of photons. The throughput which can be estimated from  $\frac{1}{c_m}$  relative to the beginning of the mission decreases to approximately 40% by the end of 2010 at low wavelengths (280 nm) while it remains above 60% at higher wavelengths (340 nm). Figure 4 shows the median throughput calculated as  $\frac{1}{c_m}$  and the m-factors  $f(\lambda)$  as  $\frac{1}{\tau}$  for channel 1 and channel 2. For this comparison the

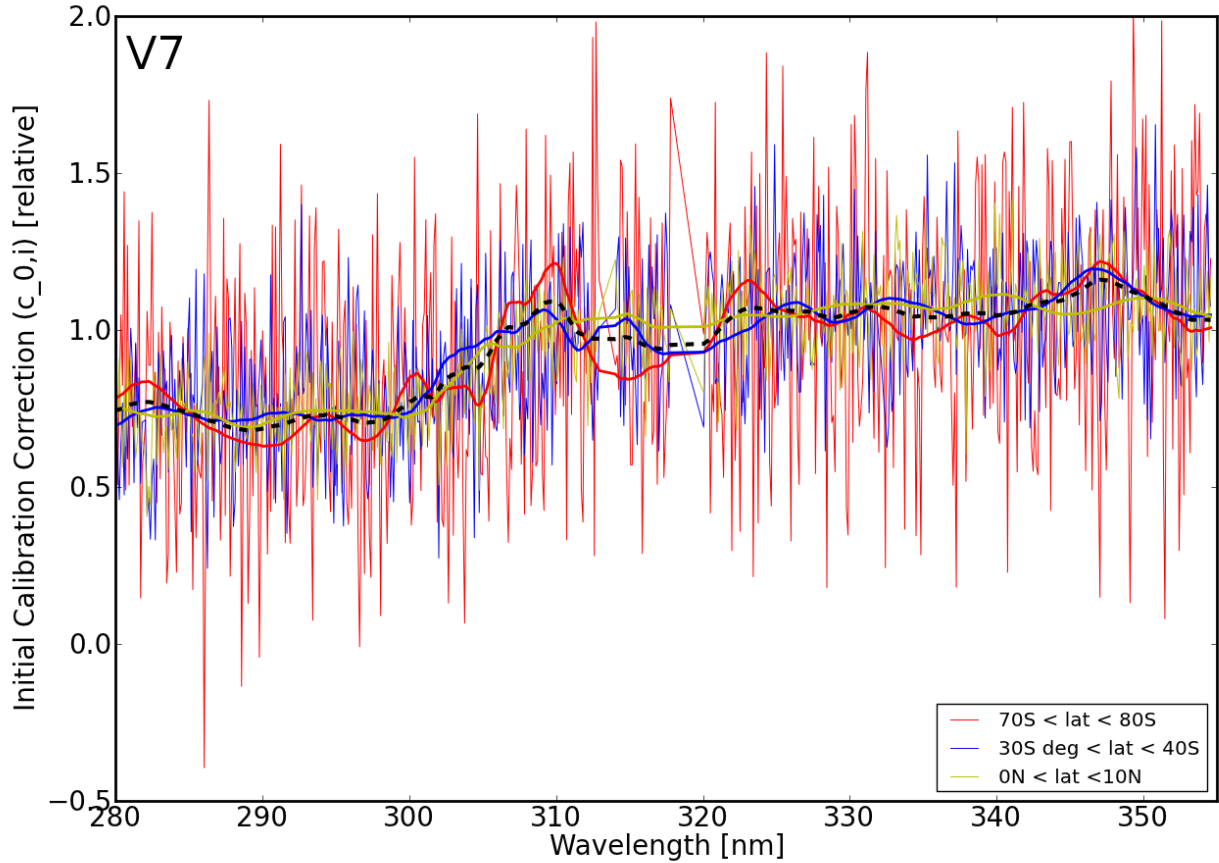


Figure 2: Initial post-launch calibration correction  $c_0$  for SCIAMACHY I1b V7 (August 2002) for the three individual geographical regions. The smoothed lines are the result of applying a 10 point boxcar. The final initial calibration correction used is shown as the black dashed curve.

m-factors were applied to the measured radiances to calculate a corrected radiance  $m_f$  using the applicator tool.  $f$  was then calculated for each region  $i$  from the  $N'$  ground pixels used to calculate  $c_{m,i}$  and averaged as

$$f(\lambda_j) = \frac{1}{3} \sum_{i=1}^3 f_i(\lambda_j) \quad (9)$$

with

$$f_i(\lambda_j) = \frac{1}{N'} \sum_{n=1}^{N'} \frac{m_{f,i,n}(\lambda_j)}{m_{i,n}(\lambda_j)} \quad (10)$$

The throughput for both datasets is comparable with far less gain seen at the end of the mission in channel 1 from  $c_m$ . Apart from these differences the agreement is to within 5%. Figure 5 shows the absolute calibration correction  $c$  for August and December from 2002 to 2012. Only two calibration corrections per year are shown to improve the readability of Figure 5. While in general radiances drop

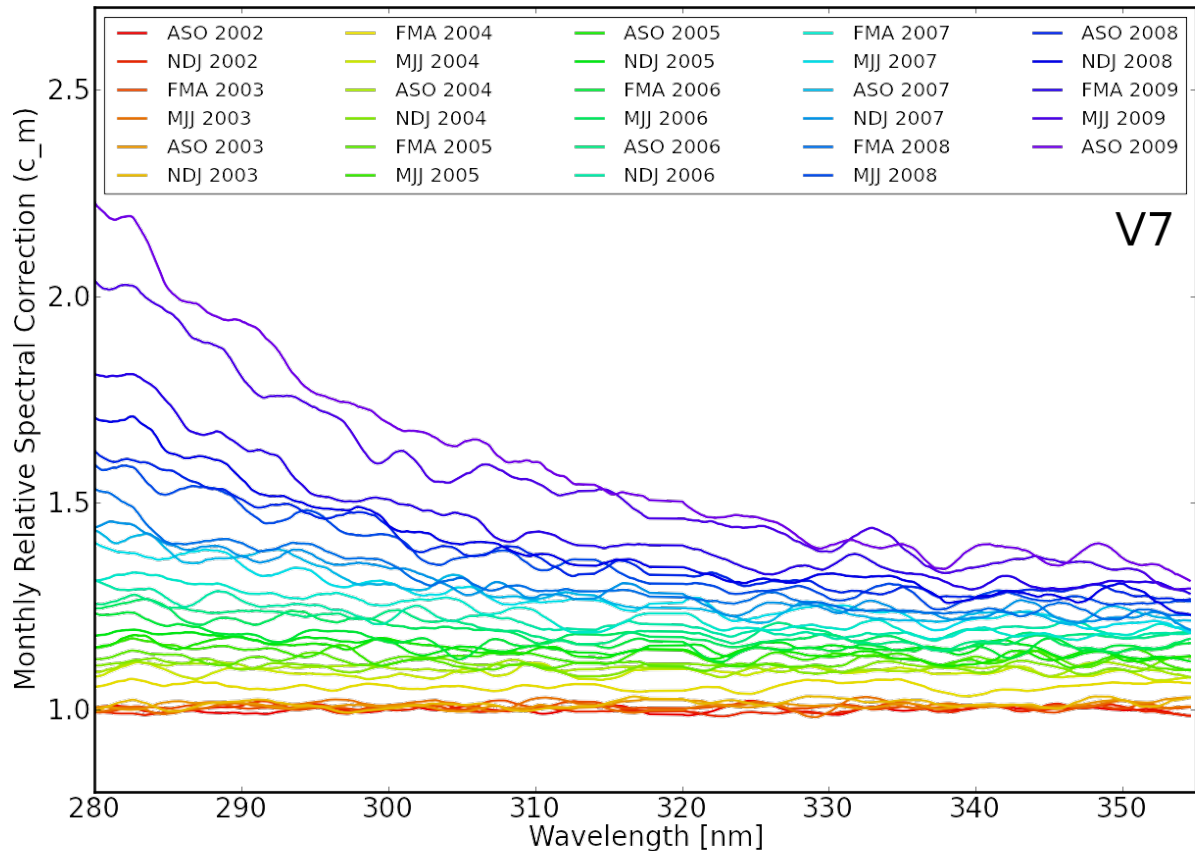


Figure 3: Monthly calibration correction  $c_m$  for SCIAMACHY I1b V7. A stronger and faster degradation is visible towards lower wavelengths.  $c_m$  is shown seasonally averaged for August to October (ASO), November to January (NDJ), February to April (FMA) and May to July (MJJ).

with time they remain fairly constant prior to 2006 with a strong decrease afterwards. No change in the radiance degradation rate means here that the degradation in the nadir spectra and sun spectra are similar. The decrease is higher in channel 1 than in channel 2. The signature of the changes from pre- to post-launch calibration is still visible throughout the years. The overall structure is in agreement with that shown in van Soest et al. (2005). In order to see how the simplified assumption on surface albedo impacts the soft calibration, tests were conducted using the albedo climatology from Koelemeijer et al. (2003). The latter is only available above 335 nm. In order to avoid sudden jumps in the albedo a Gaussian smoothing with a full width at half maximum of 3 nm was applied to the resulting albedo spectrum. The calibration differences averaged from 2002 to 2012 compared to using solely the albedos from Guzzi et al. (1996) are shown in Fig. 6. As expected no differences are visible below approximately 330 nm. At higher wavelengths there appears to be a seasonal cycle with larger differences in northern hemisphere summer. The differences are attributed to the seasonal cycle in the ice albedo in the Koelemeijer et al. (2003) climatology. In the most extreme case the difference reaches 3% but is mostly lower than 1%. It can be assumed that such differences

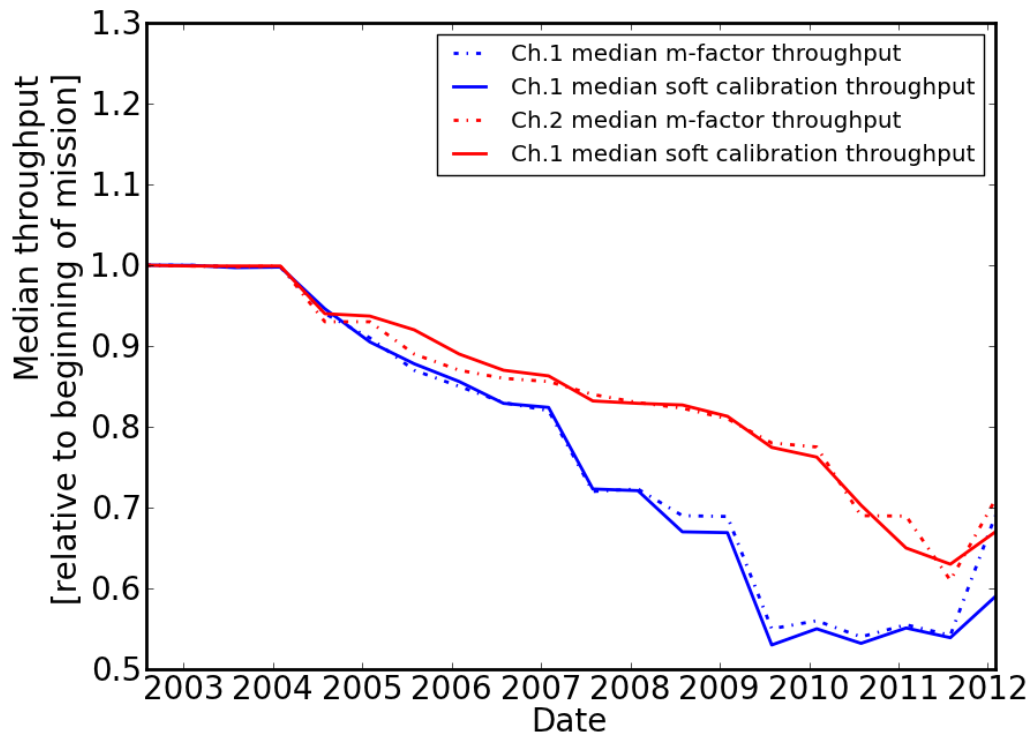


Figure 4: Median throughput for channel 1 and 2 determined from the monthly calibration correction  $c_m$  for SCIAMACHY I1b V7 and from the SCIAMACHY V7 m-factors.

will have little to no impact on retrievals performed on calibrated radiance spectra.

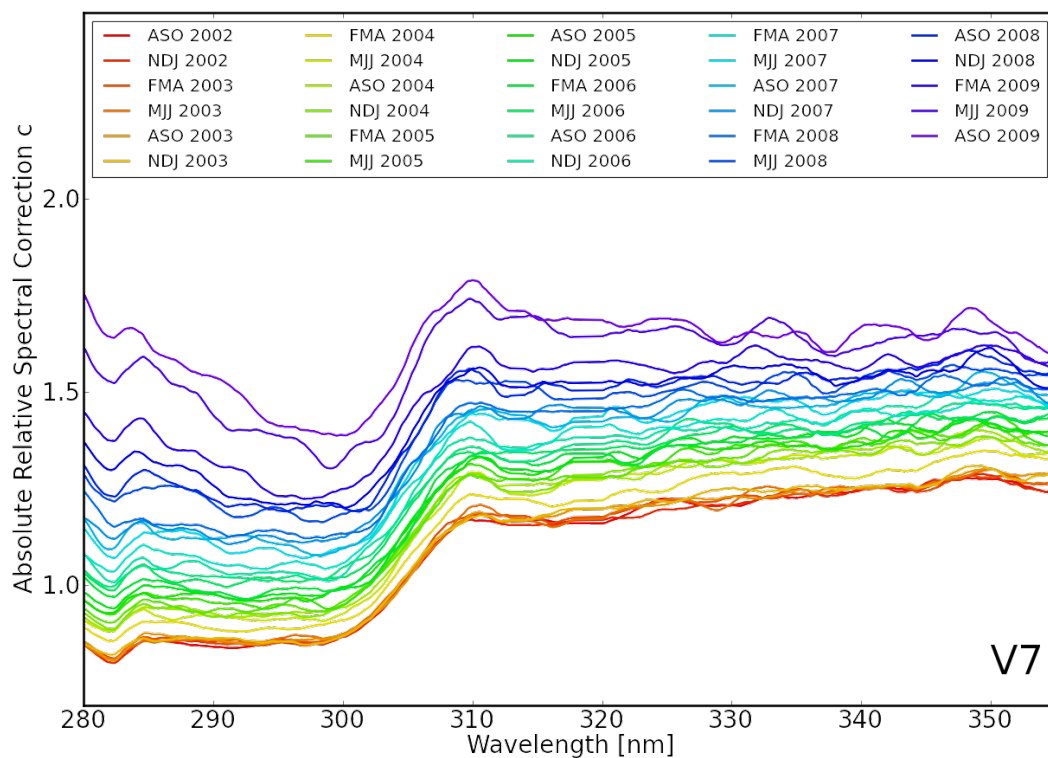


Figure 5: Evolution of the absolute calibration correction  $c$  for SCIAMACHY I1b V7. Degradation does not change much until 2004. From 2007 onwards the degradation increased again. The initial calibration can be seen as an underlying function throughout the plot and is in channel 1 larger than the degradation.  $c$  is shown seasonally averaged for August to October (ASO), November to January (NDJ), February to April (FMA) and May to July (MJJ).

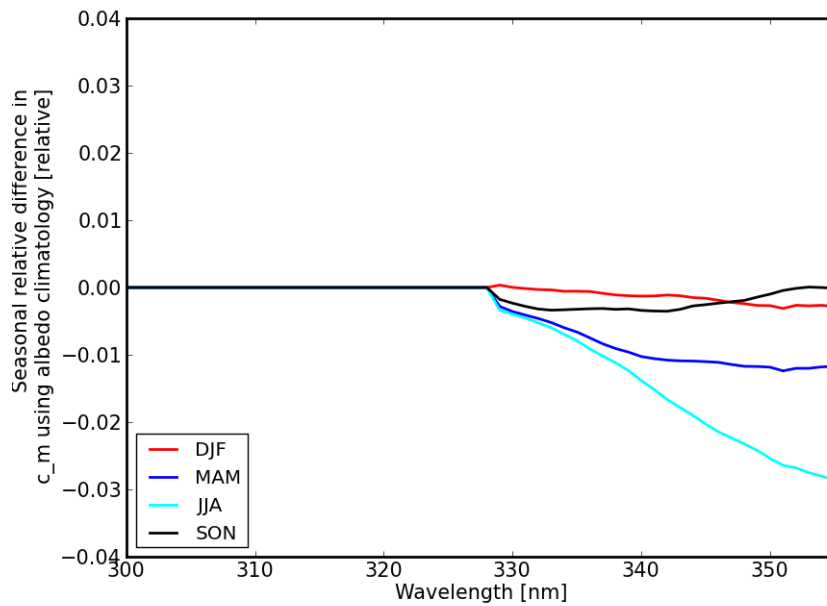


Figure 6: Differences in  $c_m$  for SCIAMACHY I1b V7 using the Koelemeijer et al. (2003) albedo climatology and using the Guzzi et al. (1996) albedos for December, January, February (red), March, April, May (blue), June, July, August (cyan) and September, October, November (black).  $c_m$  calculated using Guzzi et al. (1996) was used as the reference for calculating the relative difference.

### 3.2 Results for SCIAMACHY I1b V7 with m-factors applied

Due to SCIAMACHY V8 radiances already including a degradation correction using a mirror model (Bramstedt, 2014; Krijger et al., 2014) it is more appropriate to compare the results for V8 with results calculated for V7 with m-factors applied. In addition to the application of the m-factors additional comparison regions have been added over the Sahara (15N-30N and 0E - 25E) and central Australia (28S - 22S and 123E - 135E). All used regions are shown in figure 7. The absolute calibration

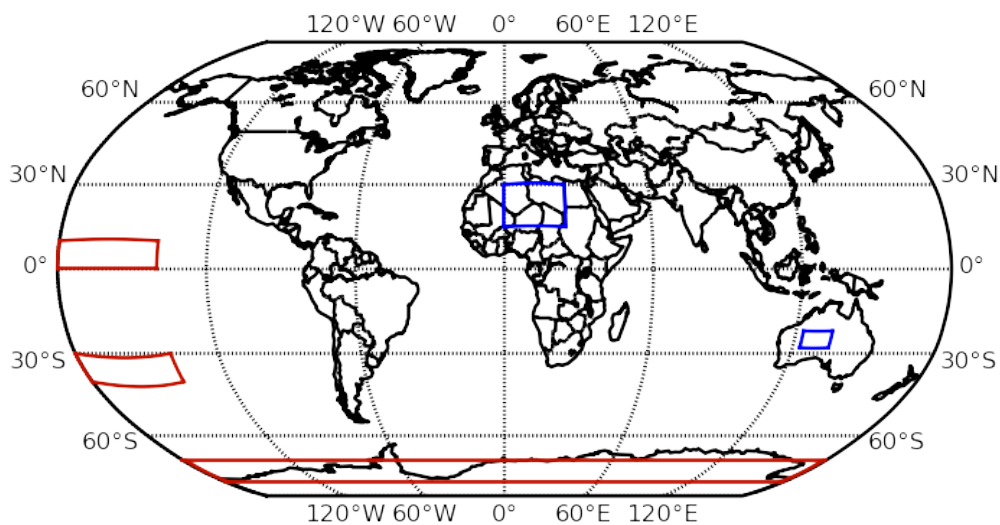


Figure 7: Map showing the three previously used regions in red and new regions in blue.

correction  $c$  is shown in figure 8. The overall structure of  $c_0$  is still visible as is expected due to the way m-factors are defined. This also indicates that the newly added regions behave in a very similar manner to the previously used regions. The monthly calibration correction  $c_m$  shown in figure 9 indicates that large parts of the degradation is countered by the m-factors. However there still seems to be some degradation, particularly below 300 nm, which is not fully handled by the m-factors.

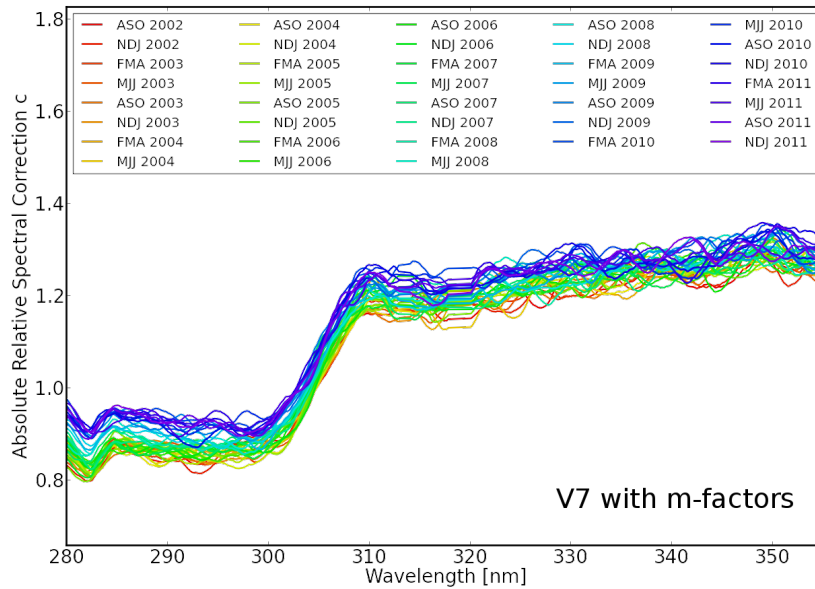


Figure 8: Evolution of the absolute calibration correction  $c$  for SCIAMACHY I1b V7 with m-factors applied.  $c$  is shown seasonally averaged for August to October (ASO), November to January (NDJ), February to April (FMA) and May to July (MJJ).

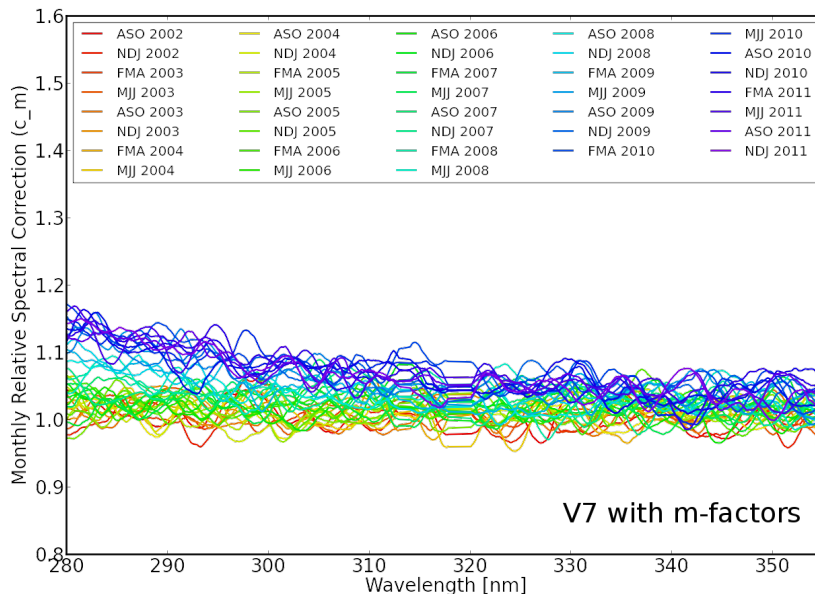


Figure 9: Monthly calibration correction  $c_m$  for SCIAMACHY I1b v7 with m-factors applied.  $c_m$  is shown seasonally averaged for August to October (ASO), November to January (NDJ), February to April (FMA) and May to July (MJJ).

## 4 Results for SCIAMACHY V8 radiances

Figure 10 shows the initial calibration correction  $c_0$  for both V7 and V8. Overall there appear to be far less spectral structures in V8. The general discrepancy between Channel 1 and 2 however remains. The relative difference between both datasets shown in figure 11 shows a few peaks in the difference around 10% with most difference below 5%. A very large shift from  $\approx -9\%$  to  $\approx 14\%$  is evident in the region from 280 to 290 nm.

The monthly calibration correction  $c_m$  is shown in figure 12 and the relative difference between V7 and V8 is plotted in figure 13. The additional degradation at lower wavelengths is much less pronounced at lower wavelengths. In addition a slight dip can be seen around 310 nm and another one at 340 nm. Three general features can be seen in figure 13.  $c_m$  is lower for V8 than for V7 with a decrease with decreasing wavelength and year indicating that the additional degradation seen in figure 9 is handled well in V8. An increasing dip in  $c_m$  for V8 vs. V7 can be seen for 310 nm - 335 nm and above 340 nm. In addition  $c_m$  appears much smoother which may also be due to the change in degradation handling.

Figures 14 and 15 show the absolute calibration correction for V8 data and its relative difference from V7 to V8 respectively. Both the features between 310 and 338 nm and above 340 nm, already evident in  $c_m$ , can be found in figure 15 indicating that most changes above 310 nm can be primarily attributed to changes over time, such as changes in the degradation handling. Furthermore a strong decrease in  $c$  can be found below 285 nm. This difference is very prominent throughout the investigated time series pointing primarily to a change in the initial measurements.

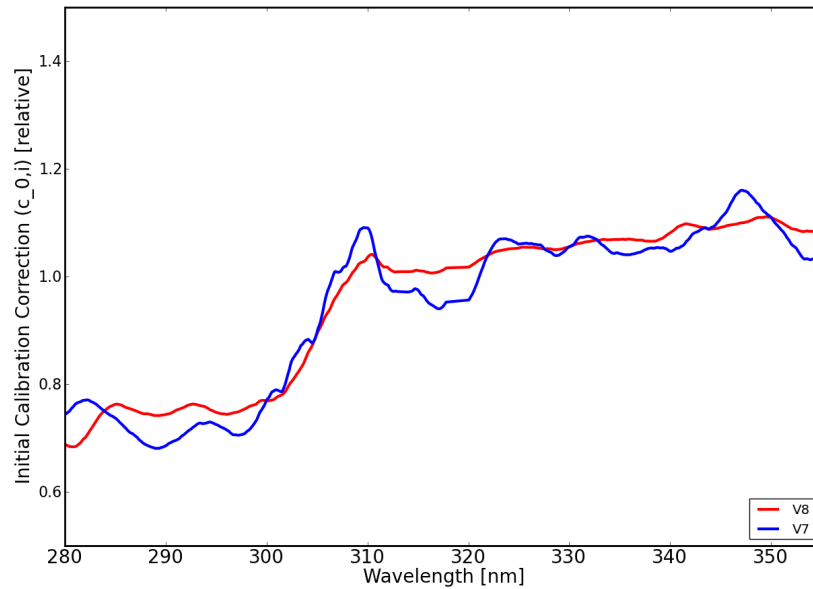


Figure 10: Initial calibration correction  $c_0$  for SCIAMACHY for Level 1b V7 and V8.

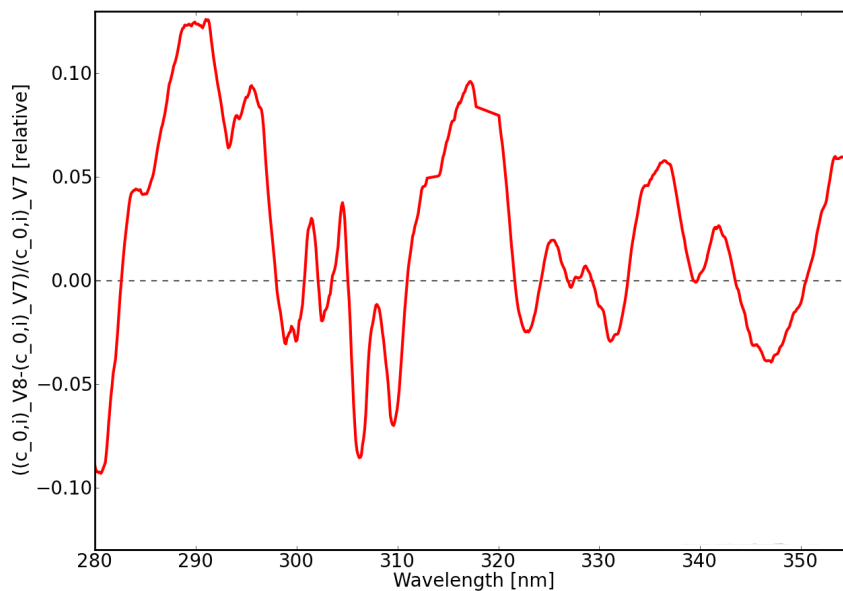


Figure 11: Relative difference in the initial calibration correction  $c_0$  for SCIAMACHY for Level 1b V7 and V8.

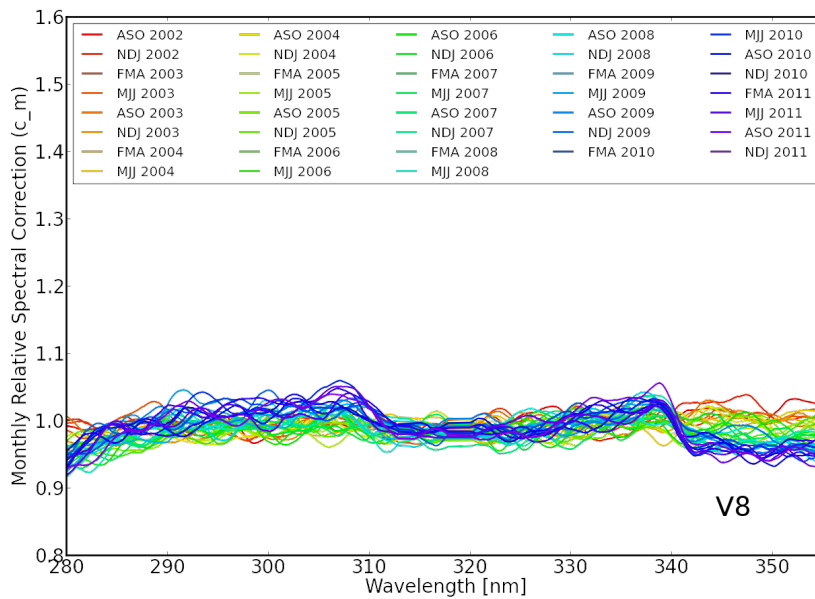


Figure 12: Monthly calibration correction  $c_m$  for SCIAMACHY I1b V8. A stronger and faster degradation is visible towards lower wavelengths. At the beginning of 2012 gains in throughput are evident.  $c_m$  is shown seasonally averaged for August to October (ASO), November to January (NDJ), February to April (FMA) and May to July (MJJ).

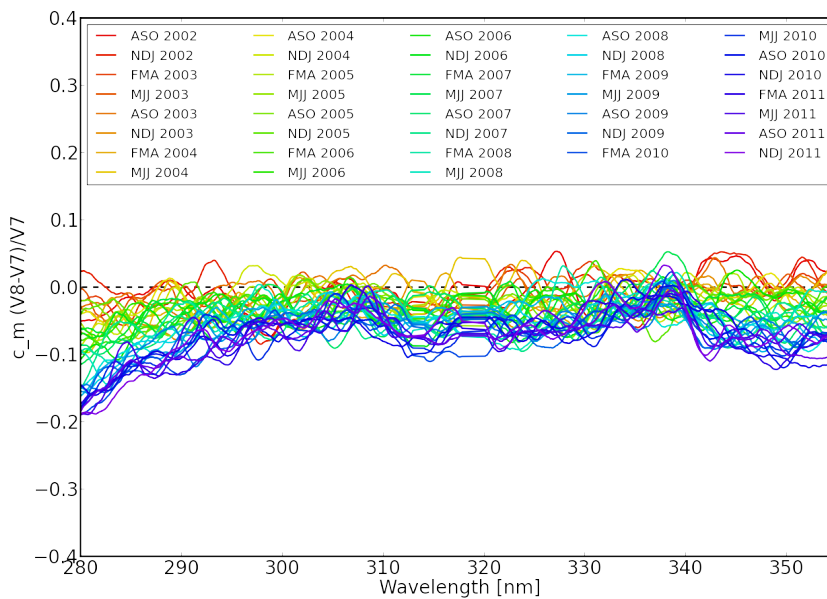


Figure 13: Relative difference in the monthly calibration correction  $c_m$  for SCIAMACHY Level 1b V7 and V8.

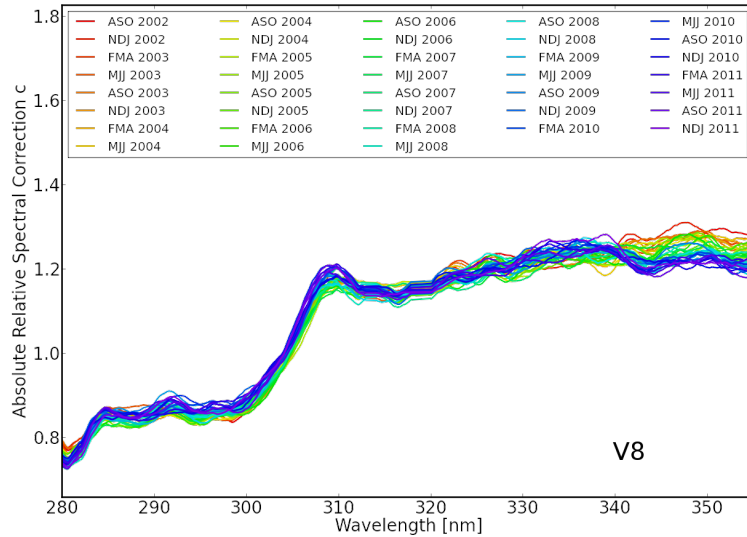


Figure 14: Evolution of the absolute calibration correction  $c$  for SCIAMACHY I1b V8. Degradation does not change much until 2004. From 2007 onwards the degradation increased again. The initial calibration can be seen as an underlying function throughout the plot and is in channel 1 larger than the degradation.  $c$  is shown seasonally averaged for August to October (ASO), November to January (NDJ), February to April (FMA) and May to July (MJJ).

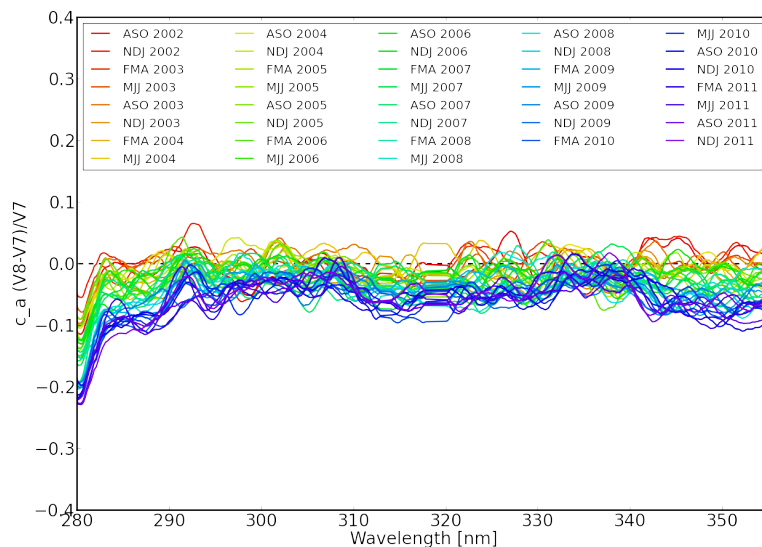


Figure 15: Relative difference in the evolution of the absolute calibration correction  $c$  for SCIAMACHY Level 1b V7 and V8.

## 5 Comparisons between V7 and V8 based on different scan-angles

For instruments like SCIAMACHY which use a scan-mirror to scan across the ground swath a scan-angle dependent degradation is expected as shown in Krijger et al. (2007). A similar behavior is also expected to occur in SCIAMACHY radiances. In the following sections the scan-angle dependent soft calibration will therefore be examined between 310 nm and 355 nm. In this wavelength region the soft calibration is conducted based on an integration time of 1s leading to 4 distinct ground pixels per scan labeled 1 to 4 from east to west. The results of the soft calibration for these ground pixels are shown in figures 16 to 27. For both datasets a stronger degradation can be seen for ground scenes further to the west with a difference to the mean degradation of up to 5% in V7. This deviation is reduced for version 8 to approximately below 3%.

### 5.1 Ground pixel no. 1

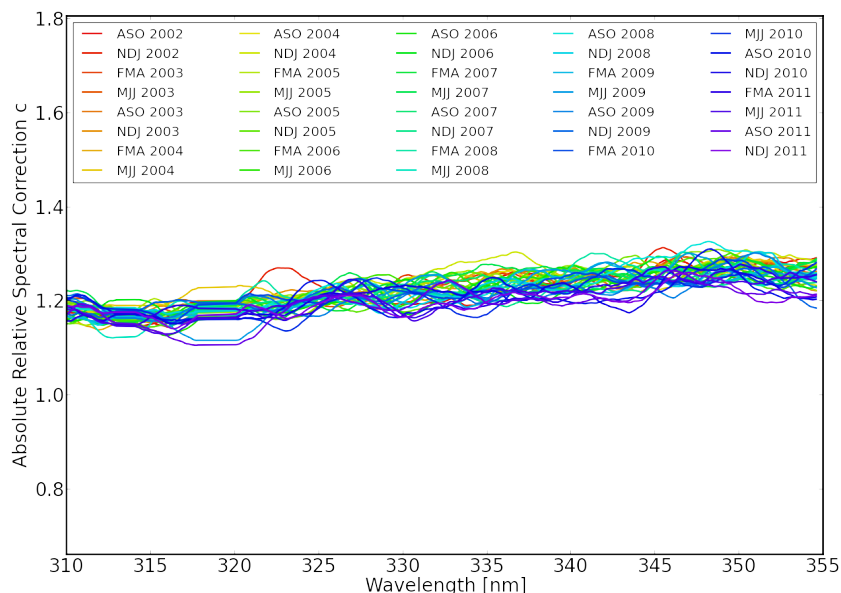


Figure 16: Evolution of the absolute calibration correction  $c$  for SCIAMACHY I1b V7 for ground pixel number 1

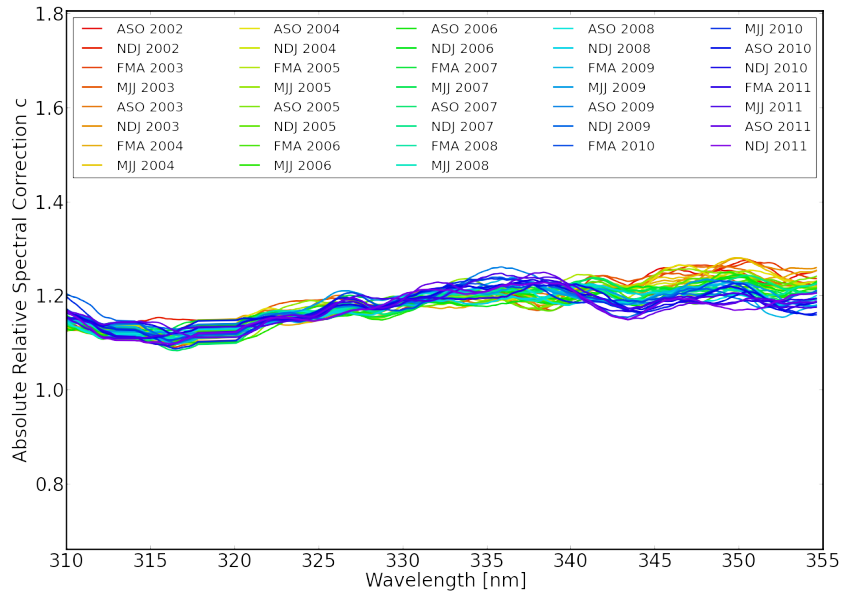


Figure 17: Evolution of the absolute calibration correction  $c$  for SCIAMACHY I1b V8 for ground pixel number 1.

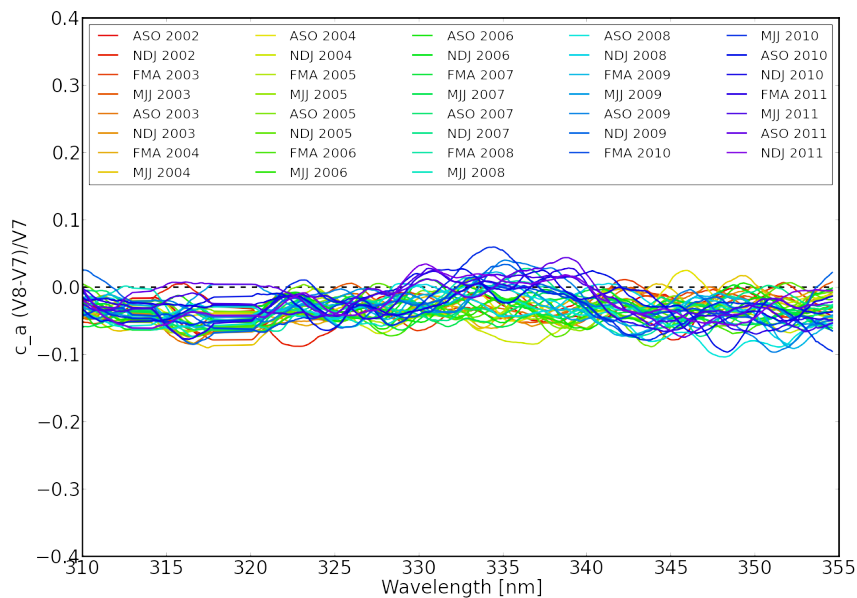


Figure 18: Relative difference in the evolution of the absolute calibration correction  $c$  for SCIAMACHY Level 1b V7 and V8 for ground pixel number 1.

## 5.2 Ground pixel no. 2

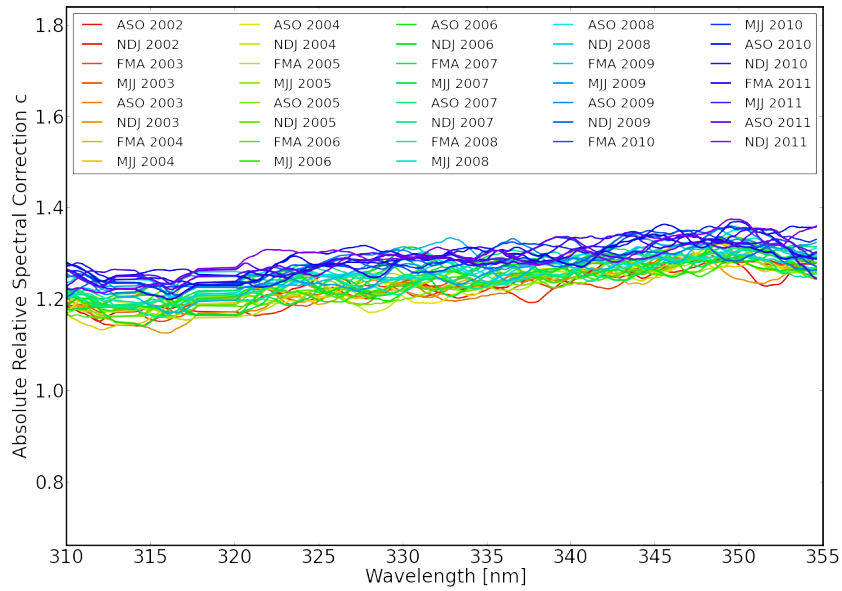


Figure 19: Evolution of the absolute calibration correction  $c$  for SCIAMACHY I1b V7 for ground pixel number 2

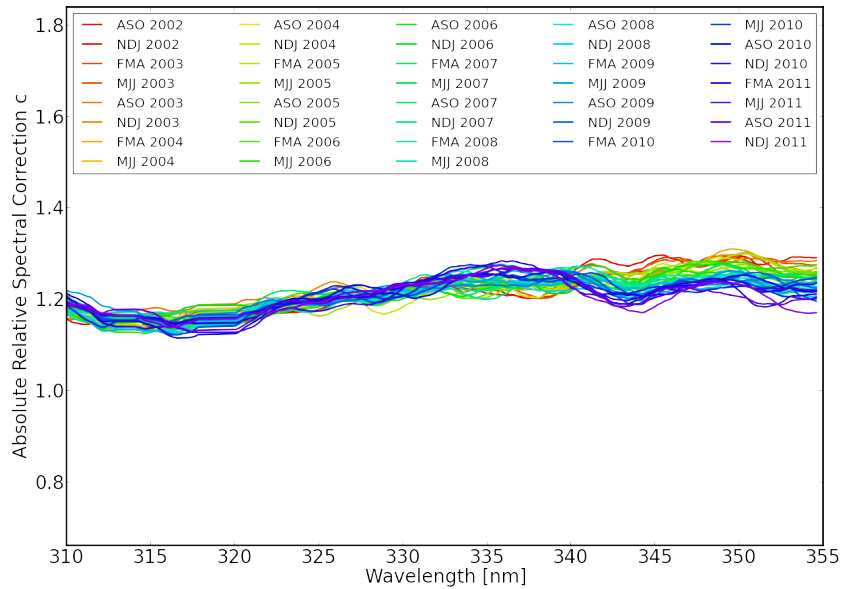


Figure 20: Evolution of the absolute calibration correction  $c$  for SCIAMACHY I1b V8 for ground pixel number 2

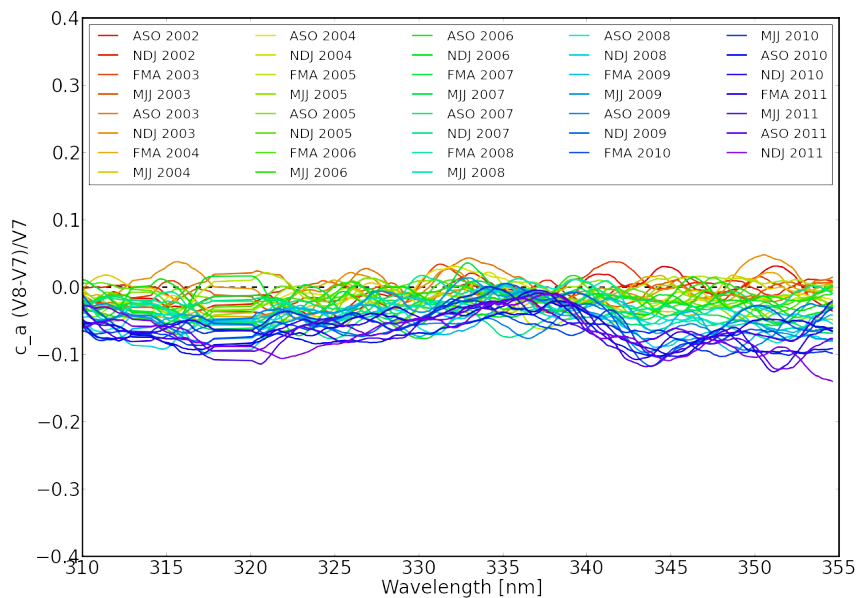


Figure 21: Relative difference in the evolution of the absolute calibration correction  $c$  for SCIAMACHY Level 1b V7 and V8 for ground pixel number 2.

### 5.3 Ground pixel no. 3

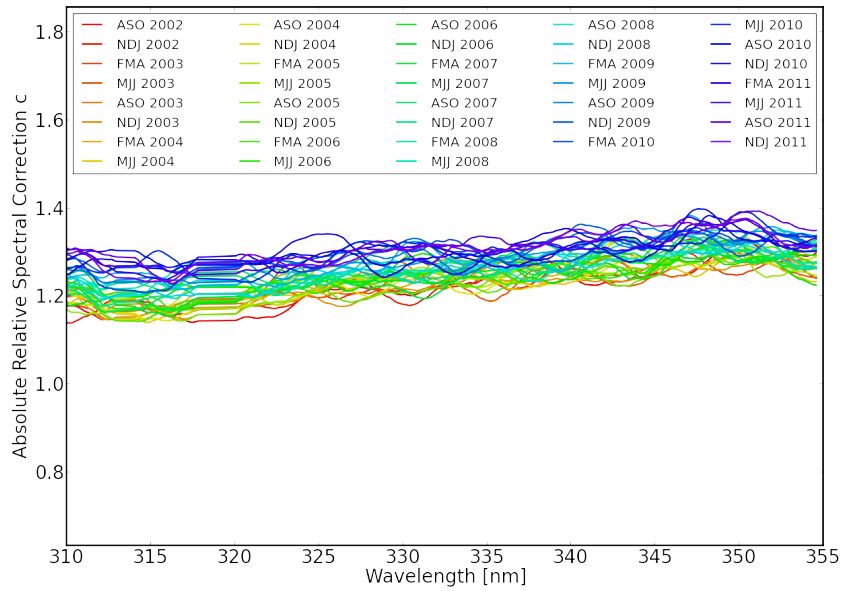


Figure 22: Evolution of the absolute calibration correction  $c$  for SCIAMACHY I1b V7 for ground pixel number 3

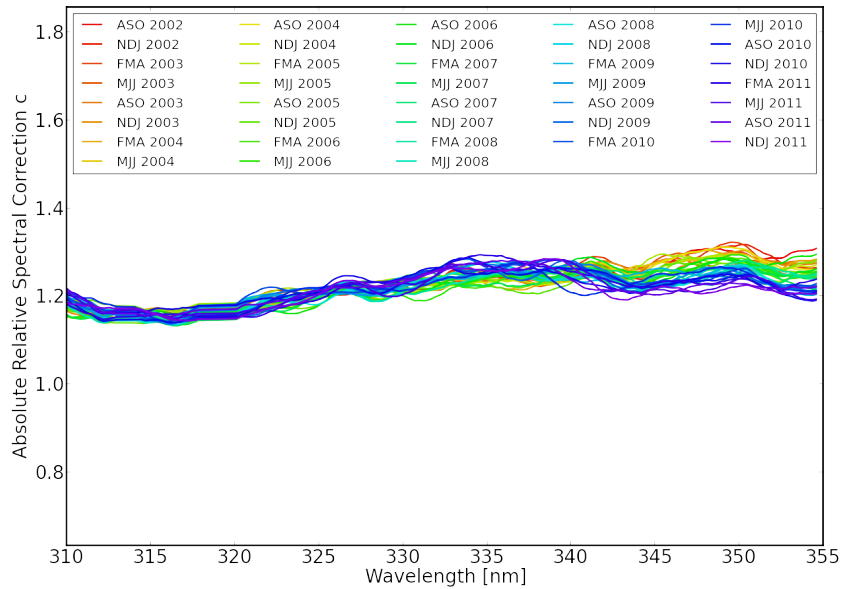


Figure 23: Evolution of the absolute calibration correction  $c$  for SCIAMACHY I1b V8 for ground pixel number 3

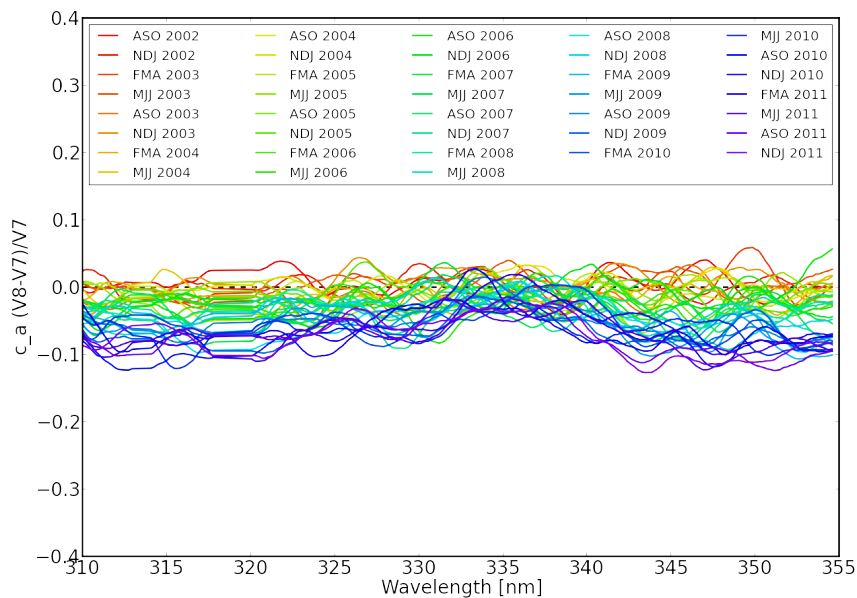


Figure 24: Relative difference in the evolution of the absolute calibration correction  $c$  for SCIAMACHY Level 1b V7 and V8 for ground pixel number 3.

### 5.4 Ground pixel no. 4

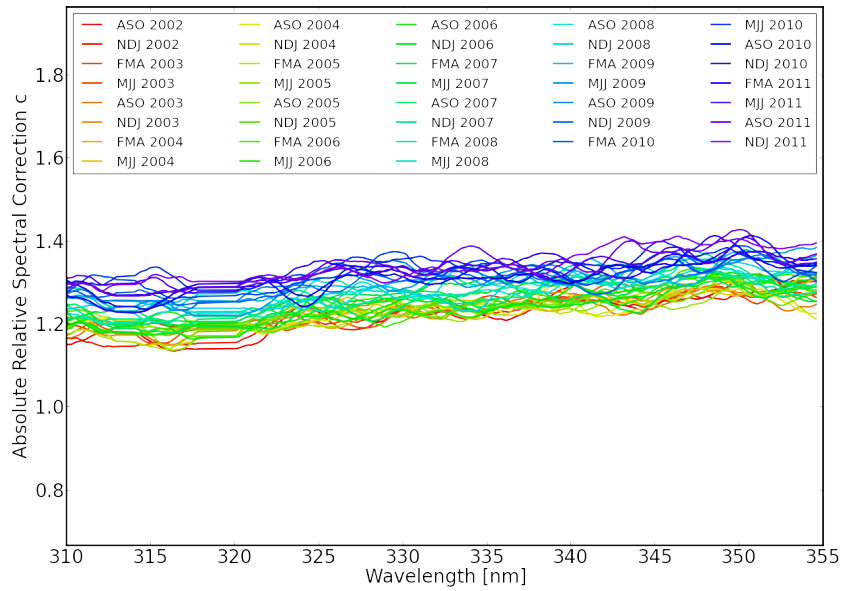


Figure 25: Evolution of the absolute calibration correction  $c$  for SCIAMACHY I1b V7 for ground pixel number 4

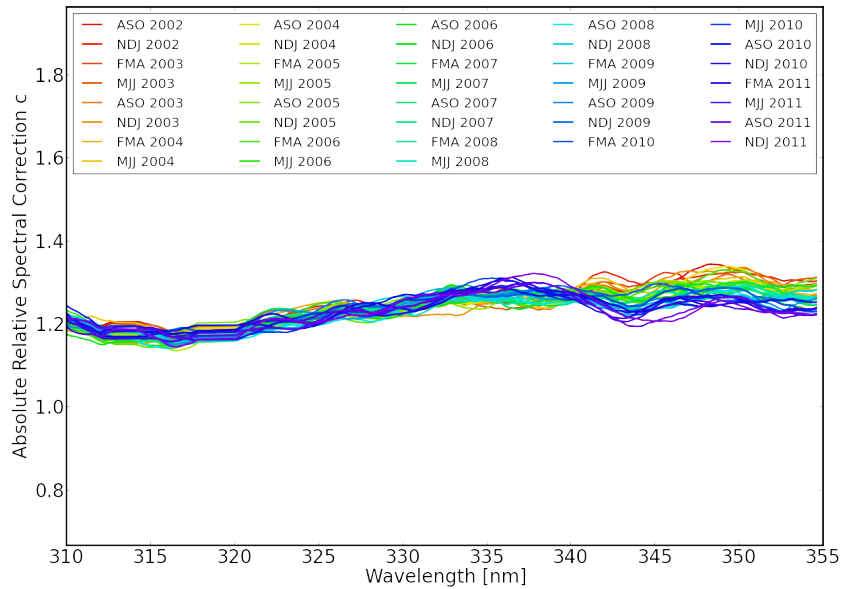


Figure 26: Evolution of the absolute calibration correction  $c$  for SCIAMACHY I1b V8 for ground pixel number 4

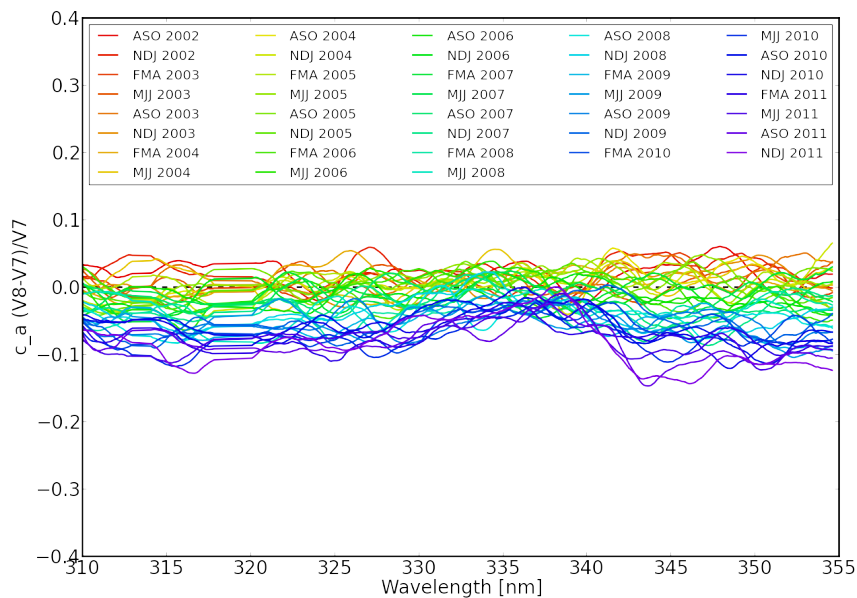


Figure 27: Relative difference in the evolution of the absolute calibration correction  $c$  for SCIAMACHY Level 1b V7 and V8 for ground pixel number 4.

## 6 Executive summary

As part of the validation and verification of SCIAMACHY V8 level 1b radiances a soft calibration approach was carried out in the wavelength range 280-355 nm. Soft calibration means here the use of radiative transfer calculated radiances with the observed total ozone (and associated profile shape from a profile climatology) as input. In order to assess differences to V7 1b radiances the same soft calibration approach was applied to V7 data and both versions directly compared. In section 3.1 it was shown that the soft calibration approach yields similar results than the m-factors with differences of within 5%. The m-factor only corrects for changes since the first radiances shortly after launch. The observed change between pre-flight and post-launch state of the instrument, as seen in section 4, show an underestimation of the radiances of about 5% to 7% between 310 and 355 nm in channel 2, while channel 1A shows an overestimation of  $\approx 20\%$  up to approximately 300 nm, which then gradually decreases in channel 1B. These effects can also be seen in version 7 which has the same underlying structure with slightly more variability. The initial recalibration (pre- to post-launch) for V7 and V8 agree to within usually 5%.

The degradation-based component of the soft calibration for V8 meaning the change since the first measurements just after launch (shown in section 4) decreases to approximately 0.92 (-8%) over a period of 9 years at 280 nm and increases to approximately 1.07 (+7%) at 309 nm. Between 309 and 312 nm the correction factor returns close to 1.0 and no degradation is evident between 312 nm and 330 nm. From 330 nm to 340 nm the degradation increases again to 5% after 9 years of operation and the degradation remains nearly constant up to 355 nm. In general the monthly soft calibration for V8 is very similar to the soft calibration results for V7 with m-factors applied. The smaller spread of soft calibration curves for V8 here suggests that the effects of degradation are handled better in V8 than in V7 with m-factors, even though the increase in radiances seen above 340 nm is a feature that is not visible in V7 with m-factors applied.

The scan angle dependence of the degradation was investigated for an integration time of 1s above 310 nm to 355 nm leading to 4 distinct ground scenes per scan. For the east-most viewing direction (ground pixel 1) the soft calibration for V8 is decreasing by approximately 2% as compared to the mean soft calibration indicating a higher throughput for this viewing direction while for V7 there also is an additional temporal component leading to an additional decrease of approximately 2.5% after 9 years of operation. In the center eastward ground scenes (ground pixel 2) there is no change in V8 with respect to the scan mean while for V7 the temporal component shows an increase of approximately 1.5% after an initial soft calibration being lower by approximately 1.5% than the scan mean. The two west-viewing ground scenes show a soft calibration which is larger than the scan mean by approximately 1-1.5% with a temporal increase by 3-4% for V7 and 1-2% for V8. The larger discrepancies are seen for the west-most viewing ground scenes.

## 7 References

- Bramstedt, K.: Calculation of SCIAMACHY m-factors, Tech. Note IFE-SCIA-TN-2007-01- CalcMFactor, 2008.
- Bramstedt, K.: Scan-angle dependent degradation correction with the scanner model approach, Tech. Note IUP-SCIA-TN-Mfactor, 2014.
- Campbell, S.: Vicarious calibration of Meteosat's infrared sensors, *ESA Journal*, 6, 151–162, 1982.
- Coldewey-Egbers, M., Weber, M., Lamsal, L. N., de Beek, R., Buchwitz, M., and Burrows, J. P.: Total ozone retrieval from GOME UV spectral data using the weighting function DOAS approach, *Atmospheric Chemistry and Physics*, 5, 1015–1025, 2005.
- Coldewey-Egbers, M., Slijkhuis, S., Aberle, B., and Loyola, D.: Long-term analysis of GOME in-flight calibration parameters and instrument degradation, *Applied Optics*, 47, 4749–4761, 2008.
- Dee, D. P., Uppala, S. M., Simmons, A. J., Berrisford, P., Poli, P., Kobayashi, S., Andrae, U., Balmaseda, M. A., Balsamo, G., Bauer, P., Bechtold, P., Beljaars, A. C. M., van de Berg, L., Bidlot, J., Bormann, N., Delsol, C., Dragani, R., Fuentes, M., Geer, A. J., Haimberger, L., Healy, S. B., Hersbach, H., Hólm, E. V., Isaksen, I., Kållberg, P., Köhler, M., Matricardi, M., McNally, A. P., Monge-Sanz, B. M., Morcrette, J.-J., Park, B.-K., Peubey, C., de Rosnay, P., Tavolato, C., Thépaut, J.-N., and Vitart, F.: The ERA-Interim reanalysis: configuration and performance of the data assimilation system, *Quarterly Journal of the Royal Meteorological Society*, 137, 553–597, 2011.
- DeLand, M. T., Huang, L. K., Taylor, S. L., McKay, C. A., Cebula, R. P., Bhartia, P. K., and McPeters, R. D.: Long-term SBUV and SBUV/2 instrument calibration for Version 8 ozone data, in: *Proceedings of the XX Quadrennial Ozone Symposium*, 2004.
- DeLand, M. T., Taylor, S. L., Huang, L. K., and Fisher, B. L.: Calibration of the SBUV version 8.6 ozone data product, *Atmospheric Measurement Techniques*, 5, 2951–2967, 2012.
- Frederick, J. E., Niu, X., and Hilsenrath, E.: An approach to the detection of long-term trends in upper stratospheric ozone from space, *Journal of Atmospheric and Oceanic Technology*, 7, 734–740, 1990.
- Gottwald, M., Krieg, E., Lichtenberg, G., Slijkhuis, S., Noël, S., Bramstedt, K., Bovensmann, H., von Savigny, C., Snel, R., and Krijger, M.: Nine years of atmospheric remote sensing with SCIAMACHY-instrument performance, in: *Geoscience and Remote Sensing Symposium (IGARSS)*, 2011 IEEE International, pp. 3538–3541, IEEE, 2011.
- Guzzi, R., Cervino, M., Torricella, F., Burrows, J. P., Kurosu, T., Rozanov, V. V., Chance, K., Watts, P., Hahne, A., and Callies, J.: A study of cloud detection, *CONTRACTOR REPORT-EUROPEAN SPACE AGENCY CR P*, 1996.
- Herman, J. R., Hudson, R. D., and Serafino, G.: Analysis of the eight-year trend in ozone depletion from empirical models of solar backscattered ultraviolet instrument degradation, *Journal of Geophysical Research: Atmospheres* (1984–2012), 95, 7403–7416, 1990.
- Herman, J. R., Hudson, R., McPeters, R., Stolarski, R., Ahmad, Z., Gu, X.-Y., Taylor, S., and Welle-meyer, C.: A new self-calibration method applied to TOMS and SBUV backscattered ultraviolet data to determine long-term global ozone change, *Journal of Geophysical Research: Atmospheres* (1984–2012), 96, 7531–7545, 1991.

- Hilsenrath, E., Bhartia, P. K., Cebula, R. P., and Wellemeyer, C. G.: Calibration and intercalibration of backscatter ultraviolet (BUV) satellite ozone data, *Advances in Space Research*, 19, 1345–1353, 1997.
- Janz, S., Hilsenrath, E., Butler, J., Heath, D. F., and Cebula, R. P.: Uncertainties in radiance calibrations of backscatter ultraviolet (BUV) instruments, *Metrologia*, 32, 637, 1995.
- Jaross, G., Cebula, R. P., DeLand, M., Steinfeld, K., McPeters, R. D., Hilsenrath, E., and Krueger, A. J.: Backscatter ultraviolet instrument solar diffuser degradation, in: *SPIE's International Symposium on Optical Science, Engineering, and Instrumentation*, pp. 432–444, International Society for Optics and Photonics, 1998.
- Koelemeijer, R. B. A., De Haan, J. F., and Stammes, P.: A database of spectral surface reflectivity in the range 335–772 nm derived from 5.5 years of GOME observations, *Journal of Geophysical Research: Atmospheres* (1984–2012), 108, 2003.
- Kondratiev, K. Y., Mironova, Z. F., and Otto, A. N.: Spectral albedo of natural surfaces, *Pure and Applied Geophysics*, 59, 207–216, 1964.
- Krijger, J. M., Aben, I., and Landgraf, J.: CHEOPS-GOME: WP2. 1: Study of instrument degradation, ESA SRON-EOS: RP/05-018 Tech. rep, 2005.
- Krijger, J. M., Snel, R., Aben, I., and Landgraf, J.: Absolute calibration and degradation of SCIAMACHY/GOME reflectances, in: *Proceedings of the Envisat Symposium*, 2007.
- Krijger, J. M., Snel, R., Harten, G. v., Rietjens, J. H. H. ., and Aben, I.: Mirror contamination in space I: mirror modelling, *Atmospheric Measurement Techniques*, 7, 3387–3398, 2014.
- Lamsal, L. N., Weber, M., Tellmann, S., and Burrows, J. P.: Ozone column classified climatology of ozone and temperature profiles based on ozonesonde and satellite data, *Journal of Geophysical Research: Atmospheres* (1984–2012), 109, 2004.
- Liu, X. and Chance, K. and Kurosu, T. P.: Improved ozone profile retrievals from GOME data with degradation correction in reflectance, *Atmospheric Chemistry and Physics*, 7, 1575–1583, 2007.
- Noël, S., Bovensmann, H., Skupin, J., Wuttke, M. W., Burrows, J. P., Gottwald, M., and Krieg, E.: The SCIAMACHY calibration/monitoring concept and first results, *Advances in Space Research*, 32, 2123–2128, 2003.
- Rozanov, V. V., Rozanov, A. V., Kokhanovsky, A. A., and Burrows, J. P.: Radiative transfer through terrestrial atmosphere and ocean: Software package SCIATRAN, *Journal of Quantitative Spectroscopy and Radiative Transfer*, 133, 13 – 71, 2014.
- Taylor, S. L., Cebula, R. P., Deland, M. T., Huang, L.-K., Stolarski, R. S., and McPeters, R. D.: Improved calibration of NOAA-9 and NOAA-11 SBUV/2 total ozone data using in-flight validation methods, *International Journal of Remote Sensing*, 24, 315–328, 2003.
- van Soest, G., Tilstra, L. G., and Stammes, P.: Large-scale validation of SCIAMACHY reflectance in the ultraviolet, *Atmospheric Chemistry and Physics*, 5, 2171–2180, 2005.
- Weber, M., Lamsal, L. N., Coldewey-Egbers, M., Bramstedt, K., and Burrows, J. P.: Pole-to-pole validation of GOME WFOAS total ozone with groundbased data, *Atmospheric Chemistry and Physics*, 5, 1341–1355, 2005.